ESAFORM 25 YEARS ON

Extending the potentials of draw-forging

Tanmoy Rakshit[1] · Johannes Gebhard[1] · Oliver Napierala[2] · Felix Kolpak[1] · André Schulze[1] · Oliver Hering[1] ·
A. Erman Tekkaya[1]

Abstract

Composite components combine the benefits of different materials, leading to improved product properties, enhanced resource- and energy efficiency and widening the product spectrum. Draw-forging is the unique combination of deep-drawing and cold forging, where a core material is encapsulated within a thin sheet metal blank. Previously, the basic draw-forging process only allowed covering of the shaft tip, and the covered length was limited by the maximum drawing ratio of the sheet. In this work, the different failure types, including tearing of the sheet, asymmetric encapsulation, and the development of a gap in the transition zone were investigated numerically and experimentally and the axial encapsulation length is increased significantly. The usage of anisotropic sheet material leads to a form fit and enhances the bond strength in draw-forged hybrid components. An alternative process route in which a pierced sheet is utilized to partially cover a specific section of a shaft was also developed. The process route was stabilized with a novel contoured counter holder to ensure high repeatability.

Keywords Hybrid component · Deep-drawing · Forward rod extrusion · Anisotropy · Encapsulation · Stabilization

Introduction

Lightweight design has the potential to increase resource efficiency and decrease CO2 emissions. In forming technology, this can be achieved either with a material-based lightweight design, meaning the load-appropriate replacement of a high-density material by a low-density one. The distribution of material can be also tailored to generate a lightweight component [1] using composite components. Besides increasing the specific strength, metallic composite components have the potential to increase the corrosion resistance, surface quality, and thermal and electrical properties [2]. Forming processes, such as cold extrusion, drawing and rolling have been used in the past to produce bimetallic parts [3]:

Composite forming

Forward rod composite extrusion of rotationally symmetrical copper and aluminium parts was investigated by [4] (Fig. 1a). With increasing surface enlargement, an increase in the bond strength was observed. The investigations were extended to additional material combinations like steel-copper, steel-nickel [5] and aluminium-steel as well as steel-stainless steel for composite shafts [6].

Forward hollow extrusion for joining serially arranged tubes of chromium steel and aluminium was applied by Ruge and Thomas [9]. They reported resulting bond strengths similar to the strength of the base material. Wagener and Haats [10] joined tubes of aluminium with titanium and stainless steel via forward hollow extrusion and demonstrated that the bond strength exceeds the strength of the undeformed base aluminium.

Yoshida et al. [11] generated a material bond between aluminium and steel by composite backward can extrusion. The result was a can with aluminium on the outer surface and steel on the inner surface (Fig. 1b). Yoshida et al. [12] showed that the strain rate does not influence the bond strength and revealed the presence of an intermetallic phase of $FeAl_3$ [7]. By simultaneous forward and backward can extrusion, [13] obtained a material bond of aluminium and

✉ André Schulze
andre.schulze@iul.tu-dortmund.de

1   Institute of Forming Technology and Lightweight Components (IUL), TU Dortmund University, 44227 Dortmund, Germany

2   Present Address: Hugo Miebach GmbH, Dortmunder Feld 51, 44147 Dortmund, Germany
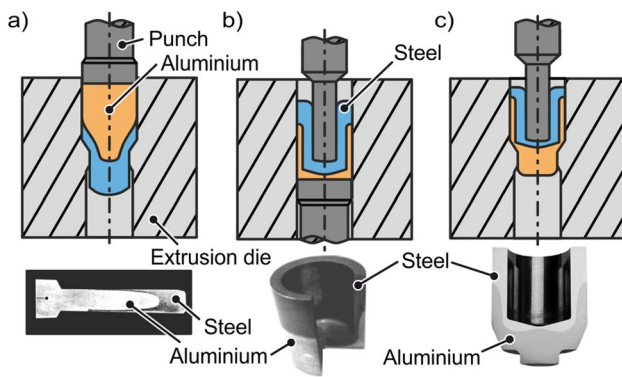
Fig. 1 Composite components produced by a) Forward rod extrusion [6] b) Backward can extrusion [7] c) Simultaneous backward can and forward rod extrusion [8]

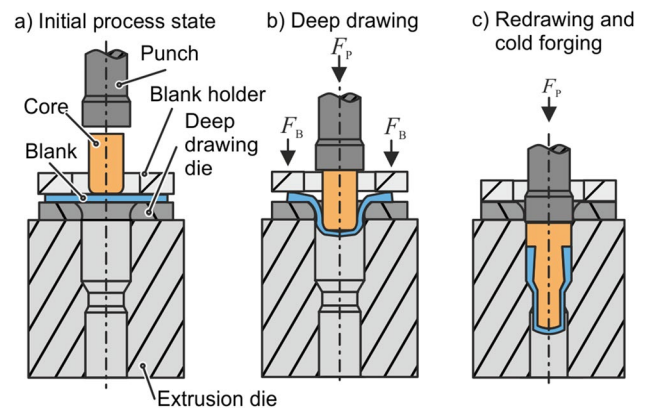**Fig. 2** Process principle of draw forging [20]

steel and showed that previous surface etching improves the resulting bond strength (Fig. 1c). [14] first formed a steel cup by backward can extrusion. An aluminium core was placed in the cup and subsequently, the hybrid part was forward extruded. They achieved both a microform-fit and a force-fit.

The joining of aluminium and steel sheets by roll-cladding was patented by the company Trierer Walzwerk [15]. In the roll cladding process, different materials are joined by a combination of pressure, surface enlargement and temperature in the roll gap [16]. The joining of tubes on solid round profiles by magnetic pulse welding was investigated by Appel and Cramer [17], who were able to join an aluminium tube with a stainless steel tube. Magnetic pulse welding is another more recent process to join semi-finished tubes. Lueg-Althoff [18] successfully joined aluminium and steel pipes. It is also possible to join interlocked semi-finished tubes by rotary swaging [19].

Draw-forging

Draw-forging is the combination of deep-drawing and forward rod extrusion in one continuous process. In the first step, the sheet is deep-drawn over a cylindrical workpiece, which initially acts as a deep-drawing punch. Subsequently, both the sheet and the cylinder are extruded simultaneously in the cold forging die (Fig. 2).

The process was invented and patented by Jäger et al. [21]. Hänisch et al. [22] investigated the process with the aim to produce single-stepped shafts with an aluminium core and a stainless steel encapsulation, but was not able to manufacture defect-free parts. Napierala et al. [23] demonstrated a successful draw-forging process with aluminium EN AW-6060 as core material and austenitic stainless steel (1.4301) for the sheet material (Fig. 3a). In further investigations process failures such as sheet fracture (Fig. 3b), the occurrence of an unwanted gap between steel and aluminium

and incomplete forming of the head were analysed and a process window was worked out [20].

An analytical model for the accurate prediction of the punch force and the ideas for further process variants were introduced. The current state of draw-forging is shown in Fig. 4a, with limited shaft encapsulation. Current research aims to enhance the encapsulated length of the shaft without changing the initial core dimensions (Fig. 4b) and to encapsulate an intermediate section of the shaft (Fig. 4c). With the existing draw-forging methodology, only a limited encapsulation of the shaft is possible. Experimental investigations revealed a maximum drawing ratio of 2. Beyond the attainable drawing ratio, the steel sheet fractured during the forward rod extrusion process
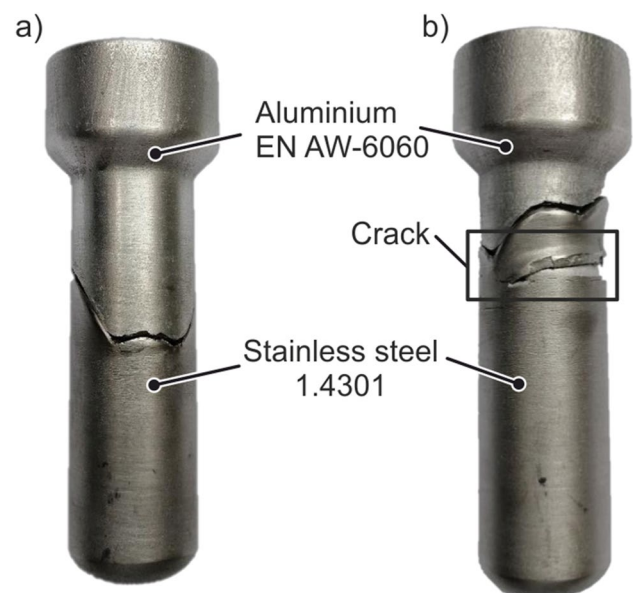
Fig. 3 a) Composite component created by draw-forging b) fracture of the sheet
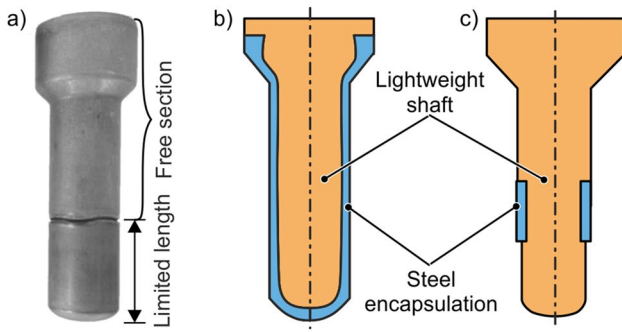
Fig. 4 a) Current state of draw-forging [20]. Enhancement through current research: b) significant increase of the encapsulated length and c) local encapsulation of an intermediate section

(Fig. 3). Similarly, a predefined local encapsulation was not possible, since circular steel sheets were used. The usage of a pierced sheet allows the local encapsulation. The external functional surface can be tailor-made based on the field of application. Electrically conductive hybrid shafts can also be produced by a local encapsulation with a conductive metal sheet. These factors create the potential to increase resource efficiency, broaden the product versatility and reduce component weight. This paper aims to resolve these limitations by introducing enhanced process variants described in the following sections.

Enhanced process principles and materials

Based on the previous limitations of the draw-forging process, two new process routes for draw-forging are developed: The first route aims to increase the encapsulated length and the second route to cover an individual section of a (multi-) stepped shaft.

Increasing *the* encapsulated length

In the original draw-forging process, the maximum encapsulated length is limited by the occurrence of sheet fracture in the drawing stage and during forward rod extrusion. To counter these limitations and prevent fracture in all process stages, the following enhancements were introduced:

1. Multi-stage deep-drawing (Fig. 5a),
2. Intermediate solution annealing of the deep-drawn cups (Fig. 5b),
3. Application of a counter pressure during forward rod extrusion (Fig. 5e).

The initial blank with the diameter d_0 is drawn to a cup with the inner diameter d_1. The deep-drawn cups are placed in a drawing die and the aluminium core with a diameter d_2 is then used as a drawing punch for redrawing. To prevent buckling of the soft core, it is supported by a centring ring (Fig. 5c). The respective drawing ratios are defined as:

$$\beta_1 = d_0/d_1, \tag{1}$$
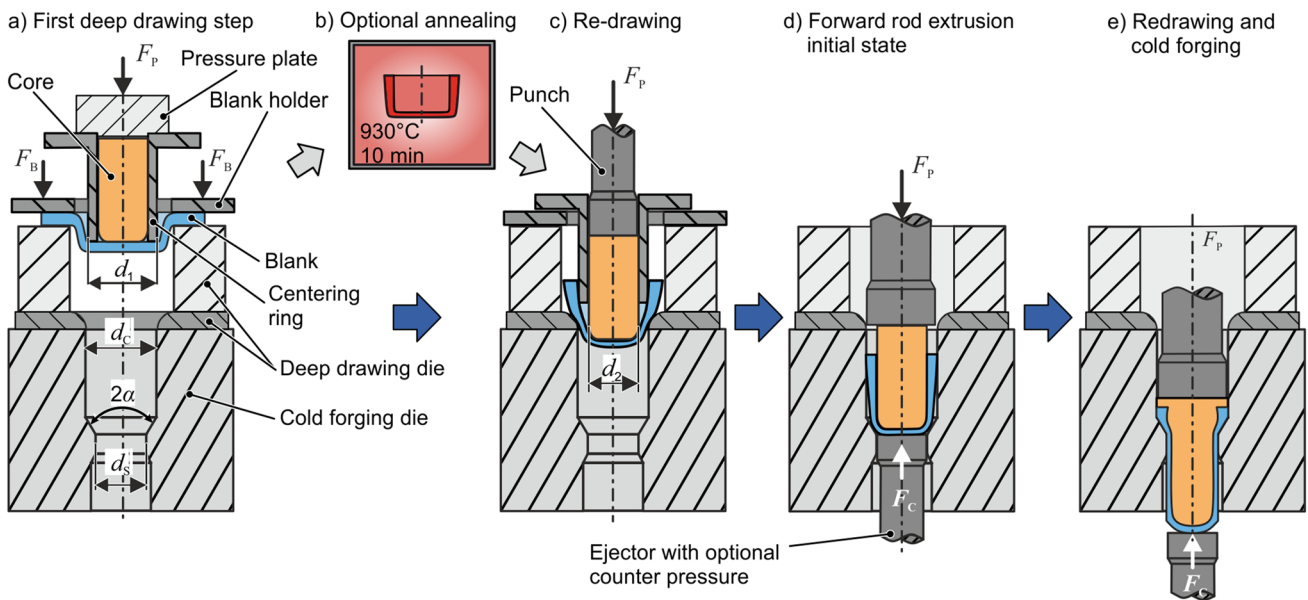
Fig. 5 New process route for the complete encapsulation of forward cold extruded parts

$$\beta_2 = d_1/d_2, \tag{2}$$

$$\beta_{12} = \beta_1 \bullet \beta_2 = d_0/d_2. \tag{3}$$

In between the initial drawing and the redrawing stage, the possibility of a solution annealing at 930 °C for 10 min was investigated to maximize the achievable drawing ratios. Though this is in contrast with the idea of a single stroke process combination of deep-drawing and cold forging, it was expected to increase the process limit significantly.

In the final step (Fig. 5e), the composite workpiece is cold forward extruded. In the scope of this project, the cold forging die had not been changed. To prevent fracture of the sheet during forward extrusion, the ejector is used to apply counter pressure. The relevant parameters in forward rod extrusion are the die angle 2α and die extrusion strain $\varepsilon_{ex} = \ln\left(d_c^2/d_s^2\right)$, with a constant container diameter $d_c = 30.2$ mm and a varying shaft diameter d_s. The shaft head diameter is the same as the container diameter, d_c. If not mentioned differently, all products had a constant shaft diameter of $d_s = 21.15$ mm and a constant shoulder-opening angle of $2\alpha = 90°$. The shaft head length was kept fixed to 20 mm. The core diameter d_2 is dependent on the sheet thickness, container diameter d_c and the drawing clearance (Fig. 5d). The core and the sheet were sandblasted, cleaned in an ultrasound ethanol bath and all surfaces which come into contact with the forging die, ejector and punch were lubricated with the phosphate-free "Beruforge 191" lubricant (Carl Bechem GmbH). The specimens were warmed to 80 °C before the application of the liquid lubricant. Forward rod extrusion was conducted upon drying of the external lubricant. The results of the investigations on the encapsulation of the complete part are presented in "Encapsulation of the complete component" section.

Encapsulation of local sections

In the basic draw forging process, only the tip of the shaft can be encapsulated with steel. The following process route is used to allow for a local encapsulation of a specific shaft section (also for multi-step shafts). The process route begins with the pre-forming of the core resulting in a narrowed tip diameter (Fig. 6a). The contoured core is then used as a punch for the deep-drawing of a perforated steel sheet (Fig. 6b). During this process, the inner diameter of the steel blank expands to the reduced diameter of the shaft. Deep-drawing over the broader section (Fig. 6c) occurs simultaneously. The core and the perforated sheet are then pressed further in the container of the extrusion die (Fig. 6d), where the composite forward rod extrusion takes place (Fig. 6e). The final location of the encapsulated section depends on the material flow of the hybrid component, which can be determined using finite element simulations or experimental investigations. The results on the encapsulation of local sections are presented in "Encapsulation of specific shaft sections" section.

Materials

To increase the strength and wear resistance of the surface of the composite parts, austenitic stainless steel 1.4301 sheets in cold rolled and bright annealed, 2R finish, with an initial thickness of $t = 1.5$ mm was used for all the investigations.
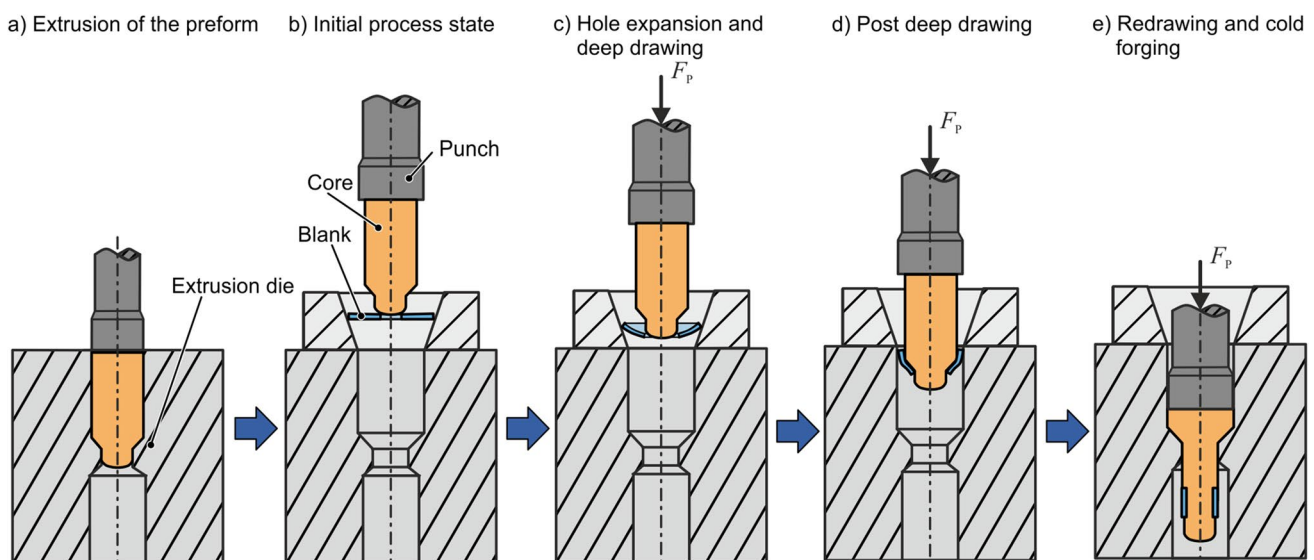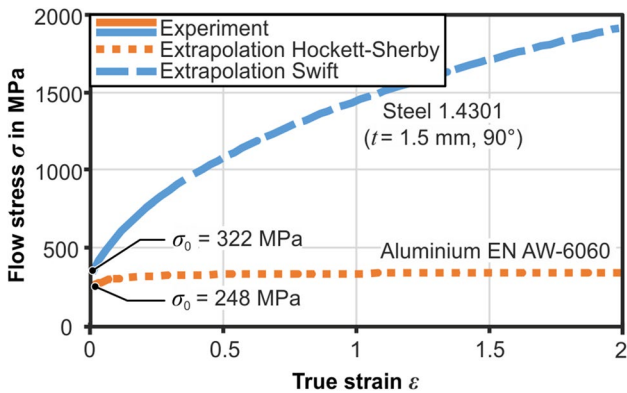

Fig. 6 Process route for encapsulation of specific section

Table 1 Chemical compositions of the workpiece materials

Aluminium AA6060 (EN 573–3)							
Si	Fe	Cu	Mn	Mg	Cr	Zn	Ti
0.30 - 0.6	0.10 - 0.30	0.10	0.10	0.35 - 0.6	0.05	0.15	0.10
Stainless steel 1.4301 (EN 10088)							
C	Si	Mn	P	S	Cr	Ni	N
0.07	1.00	2.00	0.045	0.030	17.5 - 19.5	8.0 - 0.5	0.10

Fig. 7 Flow curves of the utilized materials for draw forging

Table 2 Anisotropy coefficients of steel 1.4301

$r_{0°}$	$r_{45°}$	$r_{90°}$
0.95	1.28	0.78

The aluminium alloy AA6060 in condition T66 was used as the core material. The chemical compositions for both materials are given in Table 1.

The flow curve of the aluminium was determined in upsetting tests at room temperature. Since the flow curve of aluminium exhibits a stagnation behaviour, it was extrapolated with the Hockett-Sherby approach [24]. The flow curves of the stainless steel blank in the 0°, 45° and 90° orientations with respect to the rolling direction were determined via tensile tests at room temperature. Steel on the other hand exhibits a monotonic work hardening behaviour. Hence, the results were extrapolated with the Swift extrapolation method [25]. The resulting flow curves are given in Fig. 7.

The anisotropy parameters of the steel were implemented in the numerical models via Hill's [26] quadratic anisotropic yield criterion (Table 2). The anisotropy parameters of the Hill'48 model was identified using the plastic anisotropy ratios, r -values, obtained from the uniaxial tensile test at three different directions. This model is widely used for deep-drawing applications and has a simple parameter identification method. The approach was validated with sheet thickness measurements and measurements of the encapsulated length, shown in "Wall thickness" section.

Numerical model

The draw-forging process variants were investigated numerically with a 3D model in Simufact Forming 16.0. To capture the anisotropic behaviour of the sheet, Hill's model was implemented and the rolling direction was designated. In order to reduce the calculation time and to conduct parametric studies, a 45° section 3D model instead of a 90° model was taken. The 0° and 90° sections of the deep-drawn cups had a similar thickness and height. The material fracture starts always along the 45° section, in the region with the thinnest wall thickness. Hence, a 0° to 45° section, 1/8th model was used to simulate the deep-drawing stages and subsequent forward rod extrusion process. Both the aluminium core and the steel sheet were modelled with an elastic-plastic material behaviour. It is well established that residual stresses in forward rod extruded parts are reduced during the extrusion process [27]. Therefore, the active cold forging tools were modelled as elastic objects. All other tools were assumed rigid. The core and the sheet were meshed with tetrahedral elements. A mesh convergence study has revealed that the elements of the sheet must have a maximum edge length of 0.25 mm; the maximum edge length of the core elements was determined as 0.60 mm. Friction was modelled with the Coulomb friction model. The friction coefficient assumed for the lubricated surfaces was $\mu = 0.06$ and for the unlubricated sandblasted surfaces $\mu = 0.25$, respectively [20]. The contact surfaces between the blank and the core were not lubricated and sandblasted.

## Encapsulation of the complete component

Enhancing the process limits

The accumulated plastic strain and repeated change in the stress state leads to material fracture in the sheet metal prescribed by the critical drawing ratio. Multi-stage deep-drawing causes bending and unbending of the cups. During drawing, the cup walls experience uniaxial tensile stresses

which cause necking and thus a structural weakening. In the subsequent draw-forging, the further reduction in the wall thickness and the localization of stresses in the necked region leads to fracture of the sheet behind the die exit. To increase the encapsulated length, the goal was to maximize the total critical drawing ratio and prevent fracture in subsequent cold forging.

To enhance the process limit and prevent fracture during forward extrusion, the draw-forging process was carried out under the application of a counter holder force of $F_c = 30$ kN, which leads to a superposed hydrostatic pressure in the forming zone and thus to a reduction of critical axial tensile stresses in the sheet. Figure 8a shows the reduction of the hydrostatic stress in the steel sheet in the critical region behind the die exit where necking and fracture occurs in the experiments in terms of the stress triaxiality, defined as

$$\eta = \frac{\sigma_h}{\sigma_{\text{Mises}}}, \tag{4}$$

where σ_h is the hydrostatic or mean stress and σ_{Mises} is the von Mises effective stress. At the critical drawing ratio, the sheet fractures always along the 45° section, which is the thinnest encapsulation region in a draw-forged shaft. The material fracture can then be avoided using counter pressure to increase the hydrostatic stress in the forming zone. If the counter holder pressure is too high, the shaft is deformed below the die land making ejection impossible. Generally, the lowest necessary force should be chosen to prevent a proportional increase of the punch force. Figure 8b shows the draw-forged product with a drawing ratio $\beta_{12} = 2.22$.
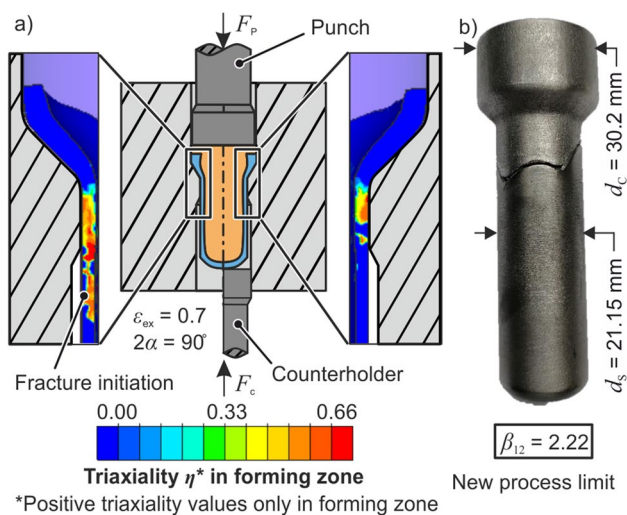
To further increase the drawing ratio and prevent fracture, solution annealing of the cups was applied between the first and second deep-drawing stage to reduce the effects of work hardening through recovery and recrystallization leading to an increase of ductility for the subsequent deep-drawing and cold forging stages. As shown in Fig. 9, the specimen with $\beta_{12} = 2.22$, has been manufactured with the applied counter holder pressure during the forward rod extrusion stage. The specimen with $\beta_{12} = 2.94$, has been manufactured using solution annealed deep-drawn cups without any counter holder pressure.

The intermediate solution annealing leads to a more significant increase of the process limit regarding the encapsulated length, even without the application of counter pressure, however, it introduces a time- and resource-intensive intermediate process step. While the mere application of counter pressure without intermediate solution annealing of the deep-drawn cups does not lead to the highest obtained drawing ratio, it does not rely on any changes of the process sequence, as the ejector is typically used to eject the part after cold forging can be directly used to apply counter pressure. Consequently, the chosen process route must be selected considering the required encapsulated length of the composite component. Both deep-drawing stages with intermittent solution annealing can be carried out separately in a batch manufacturing process. This can improve the productivity of the process in industrial applications.

In the following sections, the wall thickness distribution of the encapsulation and the bond strength between encapsulation and core are evaluated for the parts with the maximum achieved covered length.
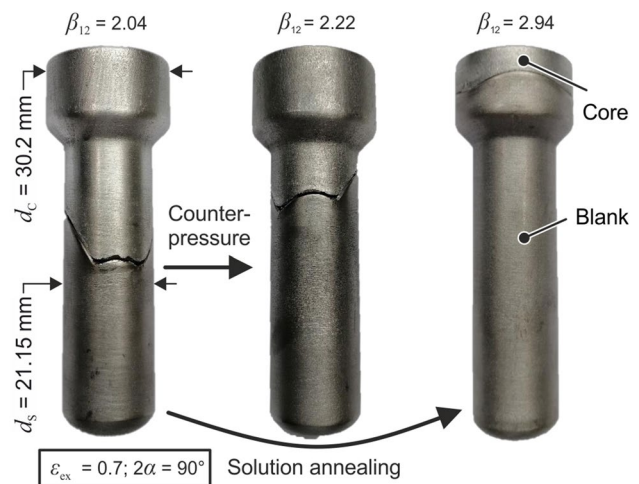

Fig. 8 a) Effect of counter pressure on the triaxiality in the steel encapsulation, b) new process limit using counter pressure during forward extrusion

Fig. 9 Increase of the initial process limit in draw forging by application of a counter-pressure or intermittent solution annealing

Wall thickness

To investigate the resulting wall thickness variation in the hybrid workpiece after extrusion, the shafts were split axially in the 0° section and in the 45° section to the rolling direction of the sheet. The numerically calculated wall thickness is 8–10% higher than the experimentally measured wall thickness. The wall thickness in the 0°-section is always larger than in 45°-section especially in the larger diameter region causing a circumferential undercut (Fig. 10). The 90°-section wall thicknesses are not shown in the figure as they are nearly identical with the values in the 0° section. The anisotropy of the steel blank causes earing during deep-drawing, leading to a beneficial form-fit in the circumferential direction, which is generated during the first deep-drawing stage and propagates further into the forward extrusion process. Apart from the transient region of the shaft, the wall thickness increases along the shaft causing an additional axial undercut and thus a macroscopic form-fit.

Bond strength

Manual sectioning of the hybrid parts revealed that no material bond of steel and aluminium was achieved, as the surface expansion necessary to break the oxides covering the aluminium surface to allow the base materials to come into mutual contact are not reached in the composite cold forging stage. Instead, a force and form-fit are the two mechanisms holding together the steel encapsulation and the aluminium core. Besides the macro form-fit described in the previous section, the sandblasting of the contacting surfaces causes a micro form-fit during forward extrusion, as the softer aluminium flows into the generated micro-cavities of the encapsulating steel sheet [14]. To evaluate the resulting local bond
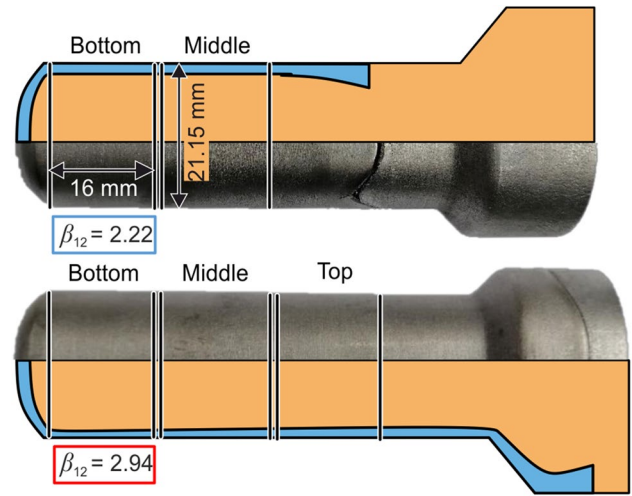

Fig. 11 Push-out test specimen extraction location

strengths between the steel encapsulation and the aluminium core, cylindrical specimens were machined out from the shaft region according to Fig. 11 to perform push-out tests. Push-out specimens with a length of 16 mm were cut using a cutting wheel with minimum feed and water cooling. The flat surfaces were then polished also with coolant to remove any remnant burrs from the machining operation.

The aluminium core was pushed out of the encapsulation to obtain force-displacement curves (Fig. 12). Due to the axial macroscopic undercut, the resulting force-displacement curves depend on the direction of the applied force, i.e. in the extrusion direction (blue curve) or against the extrusion direction (orange curve).
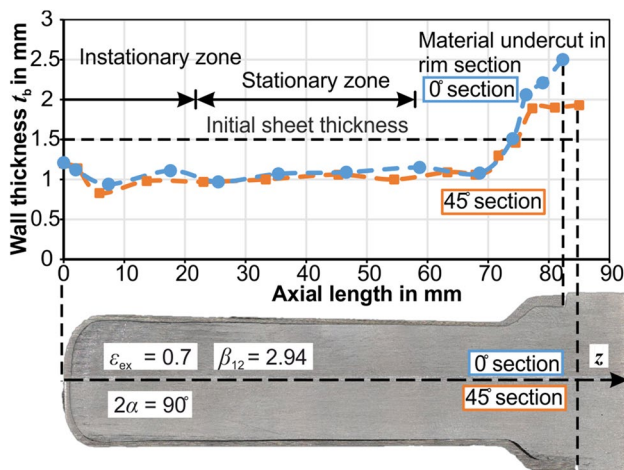

Fig. 10 Wall thickness variation for draw-forge product leading to material undercut
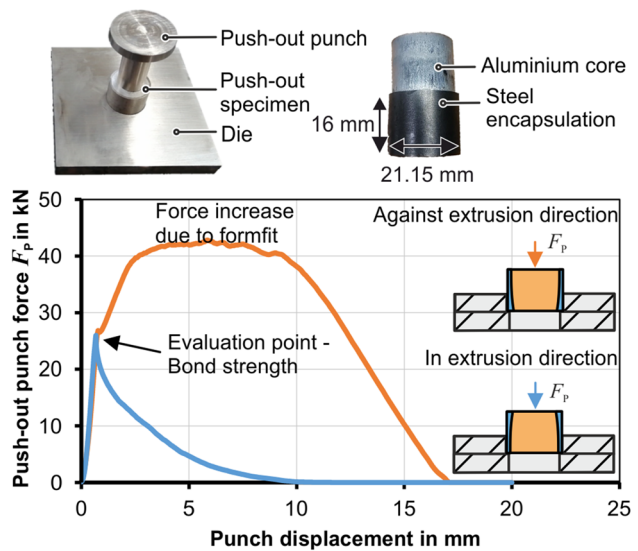

Fig. 12 Push-out test setup, resulting force-displacement curves

To evaluate only the part of the bond strength that is associated with the micro-form fit as well as the force fit, the bond strength was evaluated at the point of force drop in terms of the shear bond strength $\tau_B = F_{P,\,crit}/A_P$, where $F_{P,crit}$ is the force prior to the force drop (blue curve) and A_P is the effective contact surface between the aluminium and steel sheet. The shear bond strength was evaluated for the three aforementioned extraction regions (Fig. 13). In the case of complete encapsulation, the steel blank was solution annealed after the 1st deep-drawing stage. The resulting decrease of the bond strength in the bottom region is caused by the low plastic strain in the tip of the aluminium core leading to poor filling of the microcavities in the steel sheet during extrusion. In addition, the low sheet thickness favours elastic deformations of the encapsulation during the push-out test. Each test was repeated at least four times to account for data scattering, which was evaluated in terms of the standard deviation (error bars). The maximum attained local bond strength of 29 MPa amounts to 18% of the shear flow stress of the initial aluminium ($\tau_{max,Al} = 160$ MPa), which validates that no material bond is achieved between steel and aluminium.
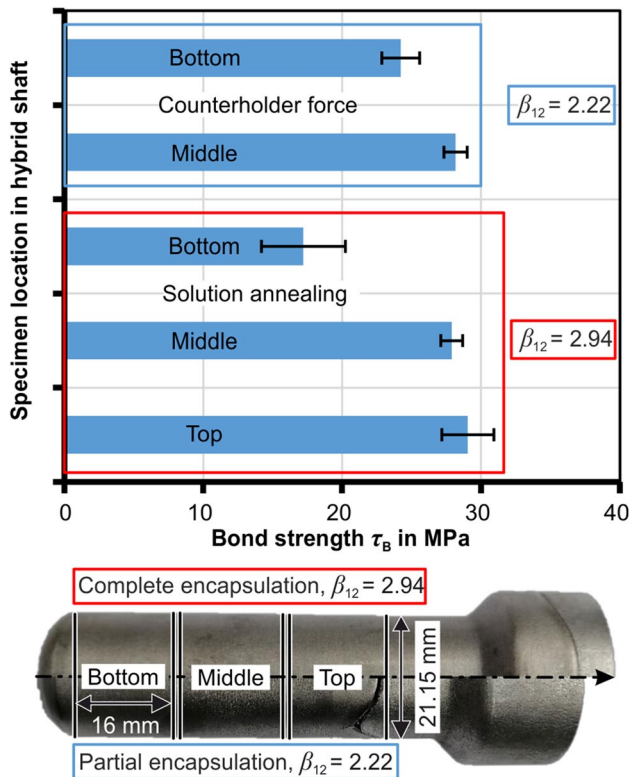

Fig. 14 Resulting gap in a) complete and b) partially encapsulated draw-forged parts

Fig. 13 Local bond strength between the aluminium core and the steel encapsulation (push-out force against the extrusion direction)
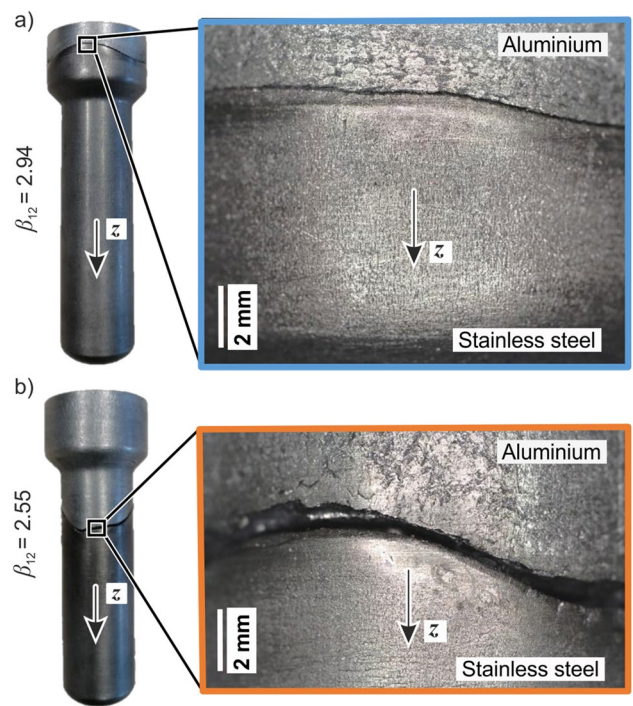
Gap generation

In the produced draw-forged parts, a gap is present between the steel encapsulation and the aluminium core. The gap is visibly larger for the partially encapsulated parts in comparison to the completely encapsulated ones (Fig. 14). The measured axial gap was 0.19 mm for the complete encapsulation and 0.95 mm for the partially encapsulated shafts. The numerical investigations revealed 0.20 mm and 0.90 mm gaps for the respective shafts. As this gap is a potential initiation point for corrosion and fracture in the potential application of the hybrid parts, its origin was investigated further.

When passing through the die shoulder, the steel sheet is pushed by the softer aluminium, preventing the generation of a gap as depicted in Fig. 15. Before the steel encapsulation leaves the extrusion die channel, it is subjected to tensile axial residual stresses, whereas the core is subjected to compressive axial stresses, as is typical for the axial residual stress distribution in forward extrusion. After the steel encapsulation leaves the die channel, the non-existent material bond between aluminium and steel allows the encapsulation to spring back and shorten axially, whereas the relieve of tensile axial stress leads the core to elongate. The combination of the two effects leads to the generation of the significant gap in the partially encapsulated parts, which can, however, be countered by encapsulating the part up to the shaft head.
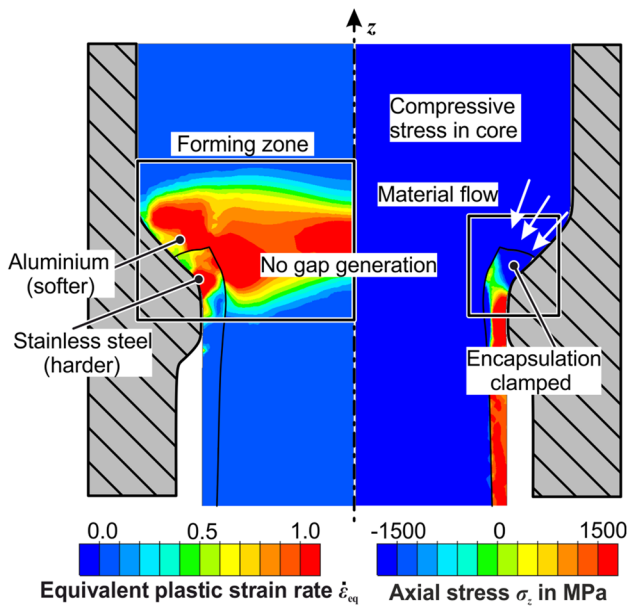
Fig. 15 Plastic strain and axial stress distribution before the steel encapsulation leaves the die channel

Encapsulation of specific shaft sections

Based on the field of application of the hybrid parts it might be beneficial to encapsulate a shaft only in a specific region. To achieve this, draw-forging was applied using hole expansion of pierced sheets (Fig. 16). To prescribe the location of the specific section after extrusion, an initially forward extruded workpiece is used. The extent of extrusion in the pre-forming stage determines the beginning of the initiation point of encapsulation in the subsequent pierced-sheet draw-forging.

To obtain a process window for the new process, the circumferential strains for inner and outer circumferential fibres of the pierced sheet were used:

$$\varepsilon_{\theta i} = \ln\left(r_{i,1}/r_{i,0}\right) \text{ and} \tag{5}$$

$$\varepsilon_{\theta o} = \ln\left(r_{o,1}/r_{o,0}\right). \tag{6}$$

Process failure types

In the application of the new process, three failure types were observed: over-expansion, under-expansion and skewed pierced sheets (Fig. 17).

A numerical parametric study was conducted using Simufact Forming 16.0 to obtain the process window of the operation. The preformed core dimensions, $r_{s1} = 21.15$ mm and $r_{s2} = 25.5$ mm, were kept constant. The shoulder opening angle for the preform was the same as
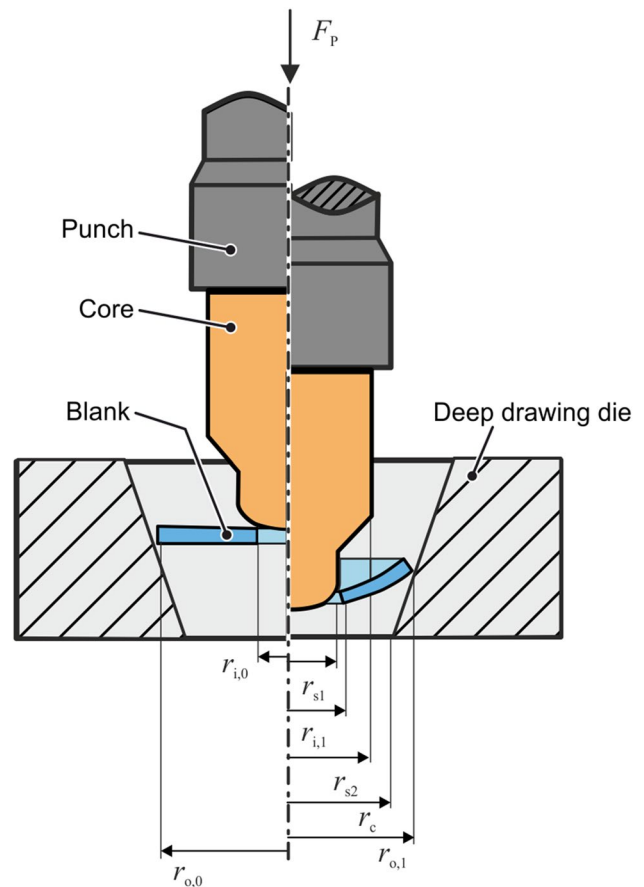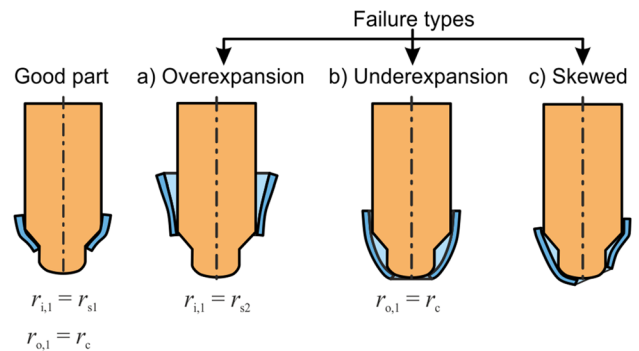

Fig. 16 Combined hole expansion and deep-drawing

Fig. 17 Failure types in pierced-sheet draw-forging

the extrusion die ($2\alpha = 90°$). The conical hole expansion and deep-drawing die had an opening angle of 22.6° and the minimum diameter is the same as the extrusion die container diameter ($d_c = 30.2$ mm). The outer and inner diameter of the stainless steel blank were the only varied parameters. Quadrilateral elements with an element edge length of 0.3 mm for the encapsulation and 0.8 mm for the preformed core were used. The deep drawing and hole

expansion tools were modelled rigid since in the deep-drawing operation the load on the tool is very low. This revealed that the sheet thickness, the clearance between the core and the extrusion die, the inner and outer sheet diameters and diameter of the stepped core determine the occurring failure type (Fig. 17).

During deep-drawing, the pierced sheet is pushed by the pre-formed aluminium core. The friction force between the core and the sheet initiates the deep-drawing and hole expansion processes. The hole is expanded over the shoulder of the preformed core. The dimension of the sheet with respect to the core dimension plays a major role in the process limits determination. Figure 18 depicts the process limits for the two deep-drawing hole expansion failure types with regard to the circumferential strains, which are prescribed by the ratio of the pierced-sheet inner and outer radii (Eqs. 5 and 6).

Experimental investigations have further revealed that the occurrence of the skewed encapsulation leads the initial process to have an extremely low success rate (Fig. 19). Out of every 20 experiments conducted, only one has led to a symmetrical encapsulation. This poor stability of the process leads to a high amount of discard and unusable conditions.

The main reason that causes skewed encapsulation is the inherent process instability. In contrast to conventional deep-drawing, where the sheet is typically clamped with a blank holder, the pierced sheet has a circumferential contact with the core and the die only at the inner and outer edges. Such boundary conditions are unstable in nature. Geometric inhomogeneity, workpiece or tool misalignment, varying frictional boundary conditions can instigate instabilities causing skewed drawing of the blank. To provoke instabilities in the numerical analysis, simulations with non-uniform friction conditions between the pierced sheet and the drawing die, modelled by the application of varying friction coefficients, were performed. The deep-drawing die was divided into four quadrants, each having a different friction coefficient, $\mu = 0.08 \pm 0.02$ (Fig. 20). A complete 3D simulation model was built up without the use of symmetry boundary
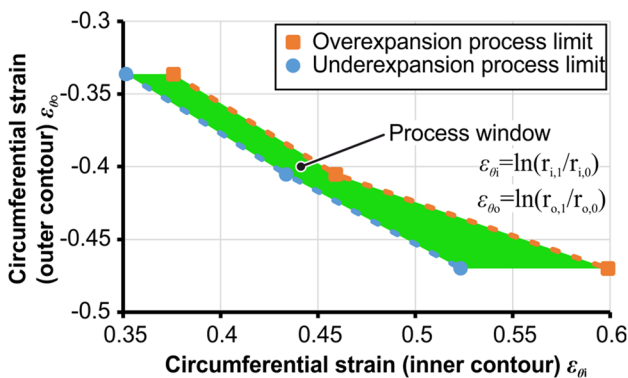

$r_{i,0} = 6$ mm
$r_{o,0} = 21$ mm
$\varepsilon_{ex} = 0.7$
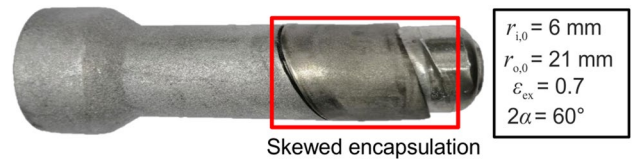$2\alpha = 60°$

Skewed encapsulation

Fig. 19 Skewed encapsulated shaft

conditions and the pierced sheet was the only deformable body. The blank had a hexahedral mesh with an element edge length of 0.5 mm. In the simulation, the prescribed friction inhomogeneity has led to an eccentric drawing of the cups similar to the observed skewed drawing in the experiments. The results underline the assumption that small deviations from perfect symmetry cause skewed sheet drawing which propagates further into the draw-forging process (Fig. 20). In the experiments, such errors are bound to occur from various sources such as manual positioning errors or imperfections in the pierced sheet or tool geometry.

Process stabilization via contoured counter holder

To stabilize the process, the degrees of freedom for the sheet had to be restricted. Hence, an additional contoured counter holder was used to pre-form the pierced sheet and fix it in place during the deep-drawing and hole expansion process (Fig. 21).

Numerical investigations have shown that the inherent process instability can be compensated with the special counter holder (Fig. 22). A parametric study, similar to "Process failure types" section, revealed that in the scope of the experimental boundary conditions, at least 30 kN counter

a) Uniform blank-die friction coefficient

b) Non-uniform blank-die friction coefficient

Core

Pierced blank

$\mu = 0.06$ $\mu = 0.09$ $\mu = 0.07$
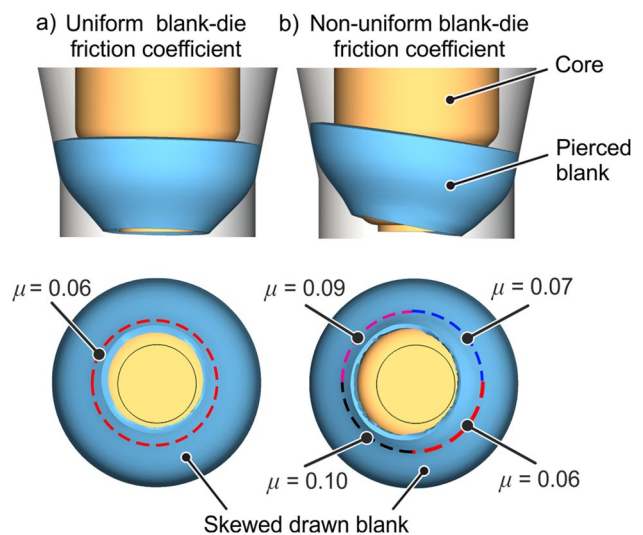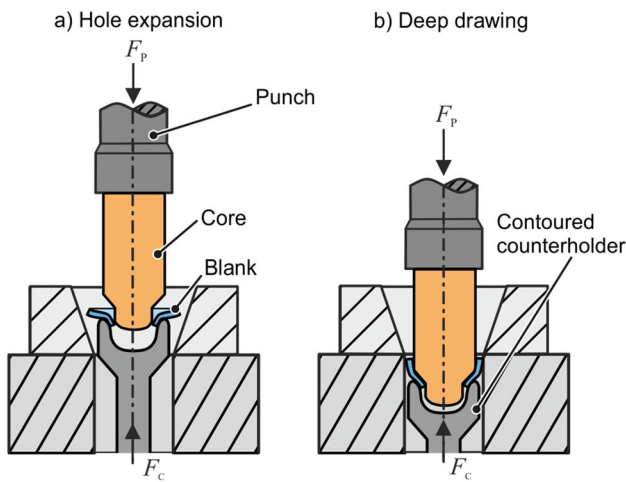
$\mu = 0.10$ $\mu = 0.06$

Skewed drawn blank

Fig. 20 Simulation of skewed cup with a) uniformly and b) non-uniformly distributed friction conditions

Fig. 18 Pierced-sheet deep-drawing limits

Overexpansion process limit
Underexpansion process limit

Process window
$\varepsilon_{\theta i} = \ln(r_{i,1}/r_{i,0})$
$\varepsilon_{\theta o} = \ln(r_{o,1}/r_{o,0})$

Circumferential strain (outer contour) $\varepsilon_{\theta o}$

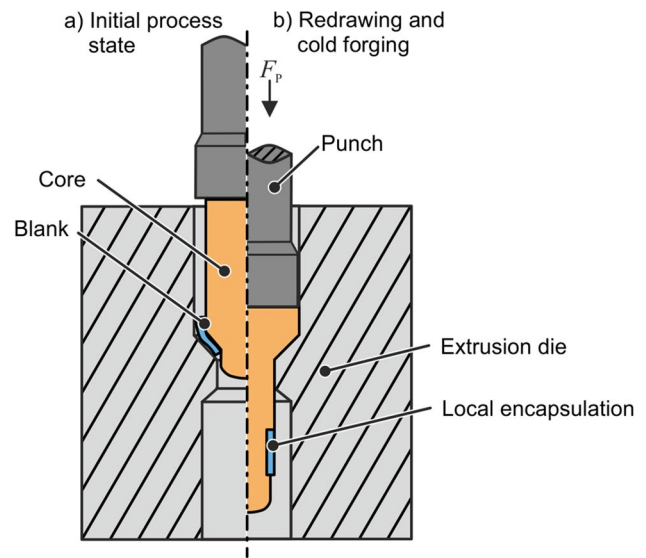Circumferential strain (inner contour) $\varepsilon_{\theta i}$

Fig. 21 Process modification with contoured counter holder for pierced sheet deep-drawing
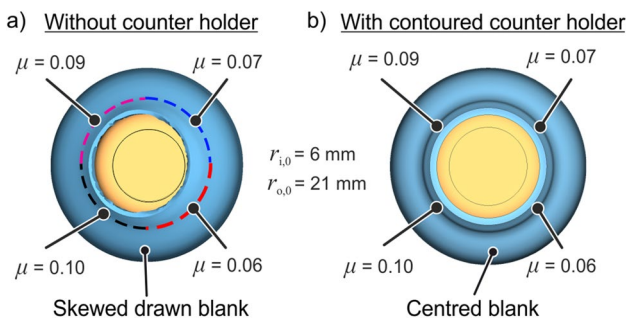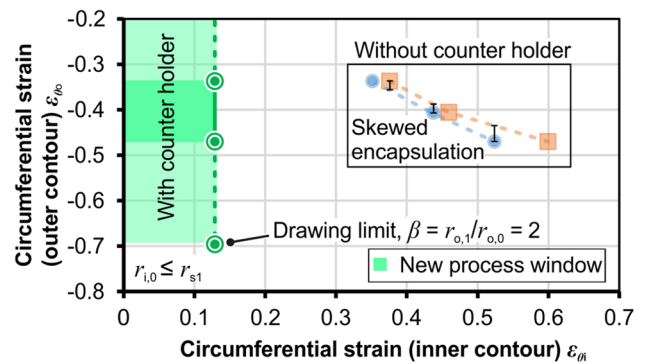

Fig. 22 a) Simulation of skewed cup drawing, b) Process stabilization by application of a contoured counter holder

Fig. 23 Local encapsulation of the core with deep-drawn pierced sheet

Fig. 24 New process window for combined hole expansion and deep-drawing utilizing a counter holder

holder force was required to prevent skewing. This force was applied on the pierced sheet and core assembly throughout the deep-drawing process. The bottom cylindrical section of the preform is a functional surface, which should not be deformed during the deep-drawing and hole expansion process. Too high counter forces can deform the softer aluminium core during the deep-drawing stage. In general, the counter force should be kept at a minimum, as it leads to a proportional increase of the punch force and the tool loads.

After deep-drawing, the aluminium core and the preformed sheet are taken out and the counter holder is removed for the forward extrusion stage (Fig. 23). For these investigations, the sandblasting of component was done after the deep-drawing stage. Which can also be done prior to deep-drawing stage, provided the deep-drawing stage be with pierced sheet having lubrication just on one side. This would eliminate the process of lubrication cleaning. The contact zone between blank and core has to remain lubricant free like in the earlier process variant. To increase the friction coefficient between the two contacting surfaces and hence

inhibit overexpansion the surface in direct contact with the core is sand blasted. The surface of the deep-drawing die is lubricated to maximize the achievable drawing ratios.

The presence of a higher clamping force, normal to the plane of sheet stabilizes the process. Most importantly, during initial forming of the sheet, it is no longer in contact with the die and thus not prone to skew. The outer diameter hence plays no role in the initial hole expansion process window as shown in Fig. 24. Further, the counter holder fixes the sheet in place and prevents the increase of the hole diameter. Hence, the three failure types do not apply to the new modified process.

In summary, the initial pierced-sheet draw forging process could be stabilized, which has resulted in a drastically increased success rate regarding the partial encapsulation of local sections by a factor of 9–10 (Fig. 25).
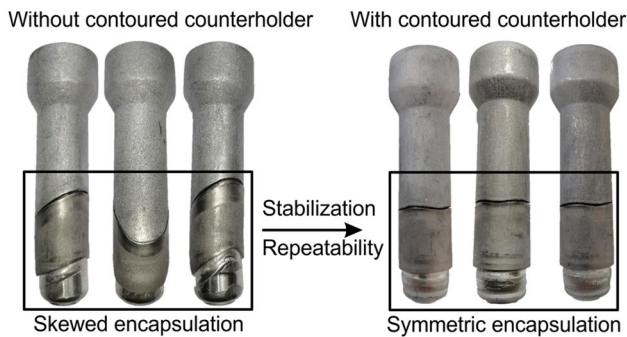
Fig. 25 Process stabilization with contoured counter holder

Conclusions

With the aim to increase the achievable product spectrum of draw-forging, two new process variants were introduced to create completely and locally encapsulated lightweight shafts with high repeatability. For both these applications, an anisotropic sheet is the most suitable option. This causes inhomogeneities in the encapsulation in the form of thickness variations and earing formation, leading to undercuts both along the axial as well as along the circumferential direction.

The process limits in the complete encapsulation of parts are enhanced significantly by the application of multiple deep-drawing stages, intermittent solution annealing of the deep-drawn cups and the application of a counter holder during forward rod extrusion preventing fracture by superposing hydrostatic pressure in the forming zone. With these measures, the maximum axial encapsulation length of the initial draw-forging process could be increased by a factor of two. It was further shown that the rolling-induced initial anisotropy of the sheet is beneficial for the bond strength of the produced hybrid components, owing to resulting variation in the wall thickness along the circumferential and axial direction after deep-drawing, which leads to an axial and circumferential form-fit during forward extrusion. Nevertheless, a material bond cannot be achieved due to the lack of sufficient surface expansion of the aluminium contact surface during forward extrusion.

Lastly, a new process was introduced to produce partially encapsulated lightweight shafts by a combination of hole expansion, deep-drawing, and subsequent draw-forging. The main failure types of the process over-expansion, under-expansion and skewed drawing were investigated numerically and experimentally. The use of a special counter holder during hole-expansion and deep-drawing was applied successfully to stabilize the process.

Declarations

References

1. Kleiner M, Geiger M, Klaus A (2003) Manufacturing of lightweight components by metal forming. CIRP Ann 52:521–542
2. Haats J (1994) Verfahrensoptimierung beim Kaltpreßschweißen artverschiedener korrosionsbeständiger Metalle, vol 305. VDI-Verlag, Düsseldorf
3. Ciupik LF (1984) Bimetallic parts production in cold backward extrusion process. Proceedings of the 17th ICFG Plenary Meeting. Nagoya, Japan
4. Gumm P, Hofmann W (1965) Kaltpreßschweißen in Fließpreßvorgängen. Int J Mater Res 56:704–712
5. Gumm P, Ruge J (1968) Kaltpreßschweißen von Stahl/Kupfer-und Nickel/Stahl-Verbundkörpern durch Fließpressen. Werkstatttechnik 58:468–471
6. Ruge J, Gumm P (1969) Kaltpreßschweißen von Verbundkörpern in Umformvorgängen. Schweißen Schneiden 21:203–209
7. Yoshida Y, Ishikawa T, Suganuma T (2014) Mechanism of forming joining on backward extrusion forged bonding process. Adv Mater Res 966-967:461–470
8. Groche P, Wohletz S, Mann A, Krech M, Monnerjahn V (2016) Conjoint forming – Technologies for Simultaneous Forming and Joining. IOP Conf Ser Mater Sci Eng 119:012025
9. Ruge J, Thomas K (1975) Kaltpresssschweißen von Rohrverbindungen aus hochlegiertem Stahl und AlMg3 in Fließpressvorgängen. Schweißen Schneiden 27:445–449
10. Wagener HW, Haats J (1994) Pressure welding of corrosion resistant metals by cold extrusion. J Mater Process Technol 45:275–280
11. Yoshida Y, Matsubara T, Yasui K, Ishikawa T, Suganuma T (2010) Influence of processing conditions on joint strength in backward extrusion forged bonding. Proceedings of the 43rd ICFG Plenary Meeting
12. Yoshida Y, Matsubara T, Yasui K, Ishikawa T, Suganuma T (2012) Influence of processing parameters on bonding conditions in backward extrusion forged bonding. Key Eng Mater 504-506:387–392
13. Wohletz S (2017) Erzeugung stoffschlüssiger Verbunde durch Kaltfließpressschweißen. Dissertation. TU Darmstadt

14. Ossenkemper S, Dahnke C, Tekkaya AE (2019) Analytical and experimental bond strength investigation of cold forged composite shafts. J Mater Process Technol 264:190–199

15. Trierer Walzwerk AG (1925) Herstellung einer Aluminiumplattierung auf Eisenblechen oder Stahlbaendern. German patent No 442131

16. Vaidyanath LR, Nicholas MG, Milner DR (1959) Pressure welding by rolling. Br Weld J 6:13–28

17. Appel L, Cramer H (2011) Magnetimpulsschweißen – Charakterisierung der Prozessbedingungen und der Verbindungseigenschaften für An-wendugen im Automotivenbereich und im Apparatebau. DVS-Berichte 275:338–345

18. Lueg-Althoff J (2019) Fügen von Rohren durch elektromagnetische Umformung –Magnetpulsschweißen. Dissertation. TU Dortmund

19. Zhang Q, Jin K, Mu D (2014) Tube/tube joining technology by using rotary swaging forming method. J Mater Process Technol 214(10):2085–2094

20. Napierala O, Dahnke C, Tekkaya AE (2019) Simultaneous deep drawing and cold forging of multi-material components: draw-forging. CIRP Ann 68:269–272

21. Jäger A, Hänisch S, Bröckerhoff S, Tekkaya AE (2011) Method for producing composite parts by means of a combination of deep drawing and impact extrusion. European patent No 2707158

22. Hänisch S, Ossenkemper S, Jäger A, Tekkaya AE (2013) Combined deep drawing and cold forging: an innovative process to manufacture composite bulk materials. Proceedings of NEMU 2013: New Developments in Forging Technology. Stuttgart, Germany

23. Napierala O, Dahnke C, Tekkaya AE (2018) Presentation of combined deep drawing and cold forging. Proceedings of the 51st ICFG Plenary Meeting. Columbus, USA. 185–192

24. Hockett JE, Sherby OD (1975) Large strain deformation of polycrystalline metals at low homologous temperatures. J Mech Phys Solids 23:87–98

25. Swift HW (1952) Plastic instability under plane stress. J Mech Phys Solids 1:1–18

26. Hill R (1948) A theory of the yielding and plastic flow of anisotropic metals. Proc R Soc Lond Ser A 193:281–297

27. Tekkaya AE, Gerhardt J, Burgdorf M (1985) Residual stresses in cold-formed workpieces. CIRP Ann 34:225–230